

Deep convolutional tensor network

Philip Blagoveschensky¹ and Anh-Huy Phan¹

¹Skolkovo institute of science and technology

June 1, 2020

Abstract

Tensor networks are linear algebraic representations of quantum many-body states based on their entanglement structure. People are exploring their applications to machine learning. Deep convolutional neural networks achieve state of the art results in computer vision and other areas. Supposedly this happens because of parameter sharing, locality, and deepness. We devise a novel tensor network based model called Deep convolutional tensor network (DCTN) for image classification, which has parameter sharing, locality, and deepness. It is based on the Entangled plaquette states (EPS) tensor network. We show how Entangled plaquette states can be implemented as a back-propagatable layer which can be used in neural networks. We test our model on FashionMNIST dataset and find that deepness increases overfitting and decreases test accuracy. Also, we find that the shallow version performs well considering its low parameter count. We discuss how hyperparameters of DCTN affect its training and overfitting.

Keywords— deep learning, convolutional neural network, CNN, deep convolutional neural network, DCNN, tensor network, EPS, entangled plaquette states, image classification, FashionMNIST

1 Introduction

Nowadays, deep neural networks achieve very good results in many machine learning tasks. One of the most important types of deep neural networks is deep convolutional neural network (**DCNN**). DCNNs achieve the best results in computer vision, image processing, video processing and fairly good results in natural language processing, time series forecasting, game playing (e.g. Checkers, Go), and other areas (PapersWithCode 2020). As identified by other researchers (Cohen, Sharir, and Shashua 2016) and by us, some of the most important characteristics that allow DCNNs to be so successful are

1. *Parameter sharing*, aka applying the same transformations to different windows of the input.
2. *Locality*. That is, interactions between nearby pixels are modeled more accurately, while interactions between far away pixels are modeled less accurately or not modeled at all. This is similar to how receptive fields in a human’s visual cortex works.
3. *Deepness*. DCNNs are deep and have a lot of parameters, which allows them to learn complicated transformations.

Tensor networks are linear algebraic representations of quantum many-body states based on their entanglement structure. Nowadays, people are exploring their applications to machine learning but are not getting as good results as with deep neural networks. One of the applications is tensor regression - a class of machine learning architectures based on contracting a (possibly preprocessed) input with a tensor network.

Our goal in this work is to devise a regression model which would have the three aforementioned characteristics of DCNNs (parameter sharing, locality, and deepness) in hope that such a model would perform as well as DCNNs. Since image classification is the most straightforward application of DCNNs, that’s the machine learning task we choose to evaluate our model on. The main contributions of this article are:

- We propose a novel tensor regression based model based on the composition of tensor networks called EPS (Entangled plaquette states) which satisfies the aforementioned three desiderata (Section 3.4)
- We show how EPS can be implemented as a backpropagatable function/layer, which can be used in neural networks or other backpropagation based models (Section 3.3).
- Using common techniques for training deep neural networks, we train and evaluate our model on FashionMNIST dataset (Xiao, Rasul, and Vollgraf 2017a). We find that while a shallow model based on one EPS is competitive with DCNNs in accuracy and parameter count, making it deeper causes more overfitting and thus worse accuracy (Section 4).
- We show how various hyperparameters affect the model’s optimization and generalization (Section 5).

2 Related work

As far as we know, some tensor networks enjoy one or two out of three desiderata (parameter sharing, locality, and weight sharing), but none have all three. For example,

- MERA (see Ch. 7 of (Bridgeman and Chubb 2017)) is a tree-like tensor network used in quantum many-body physics. It has locality and is deep, but doesn't have weight sharing.
- Deep Boltzmann machine can be viewed as a tensor network, see Sec. 4.2 of (Cichocki, Phan, et al. 2017) or (Glasser, Pancotti, and Cirac 2018) for discussion of how restricted Boltzmann machine is actually a tensor network. It's not difficult to see a DBM is a tensor network as well). For supervised learning, it can be viewed as tensor regression with deepness, but without locality or weight sharing.
- (Glasser, Pancotti, and Cirac 2018) introduces entangled plaquette states (EPS) with weight sharing for tensor regression. They combine one EPS with a linear classifier or a matrix tensor train. Such a model has locality and parameter sharing but isn't deep.
- (Cohen, Sharir, and Shashua 2016) introduces a tensor regression model called Deep convolutional arithmetic circuit. However, they use it only theoretically to analyze the expressivity of DCNNs and compare it with expressivity of tensor regression with tensor in CP format (canonical polyadic / CANDECOMP PARAFAC). Their main result is a theorem about the typical canonical rank of a tensor network used in Deep convolutional arithmetic circuit. The tensor network is extremely similar to our composition of EPSes. We conjecture that the proof of their result about the typical canonical rank being exponentially large can be slightly modified to apply to our tensor network as well.
- (Liu et al. 2019) uses a tree-like tensor regression model with all cores being unitary. Their model has locality and deepness, but no weight sharing.
- (Stoudenmire and Schwab 2016) and (Novikov, Trofimov, and Oseledets 2016) perform tensor regression on MNIST images and tabular datasets, respectively. They encode input data as rank-one tensors like we do in Section 3.2 and contract it with matrix tensor train to get predictions.

3 Description of the whole model

3.1 Copy operation in tensor networks

There are multiple introductions to tensor network diagrams available. We recommend Chapter 1 of (Bridgeman and Chubb 2017), (Ehrbar 2000) (this article doesn't call them tensor networks, but they are), and Chapter 2 of (Cichocki, Lee, et al. 2016). Other introductions, which are less accessible for machine learning practitioners, are (Orús 2014) and (Biamonte and Bergholm 2017). We extend the notion of tensor networks by introducing the **copy operation**. We call tensor networks with the copy operation **generalized tensor networks**. The copy operation was invented by (Glasser, Pancotti, and Cirac 2018). The copy operation takes a vector as input and outputs multiple copies of that vector. In generalized tensor network diagrams, we graphically depict the copy operation by a red dot with one input edge marked with an arrow, and all output edges not marked in any way. This operation is equivalent to having two copies of the input contracted with the rest of the tensor network. In order for a generalized tensor network to be well defined, it must have no directed cycles going through copy elements (if we consider the usual edges between tensors to have both directions). Figure 1 explains the copy operation in more detail.

3.2 Input preprocessing

Suppose we want to classify images with height H pixels, width W pixels, and each pixel is encoded with C color channels, each having a number in $[0, 1]$. Thus, such an image is usually represented as a tensor $X \in [0, 1]^{C \times H \times W}$. We want to represent it in another way. We will call this other way the 0th representation X_0 of the image. Throughout our work, when we will be using variables to talk about the zeroth representation of an image, we will be giving the variables names with the subscript 0, and for other representations we will be giving variables names with other subscripts. We denote $W_0 = W$, $H_0 = H$, so for some small positive integer Q_0 (where Q stands for "quantum dimension"), we want to represent the image as HW vectors, each of size Q_0 :

$$\forall h \in \{1, \dots, H\} \forall w \in \{1, \dots, W\} X_0(h, w) \in \mathbb{R}^{Q_0}.$$

In our work, we have experimented only with grayscale images (i.e. $C = 1$) and only with the 0th quantum dimension size $Q_0 = 2$, so we will describe preprocessing only for this case, and we will omit the dimension C . The usual approach to creating such a representation is to choose a vector-valued function

$$\varphi : [0, 1] \rightarrow \mathbb{R}^{Q_0}$$

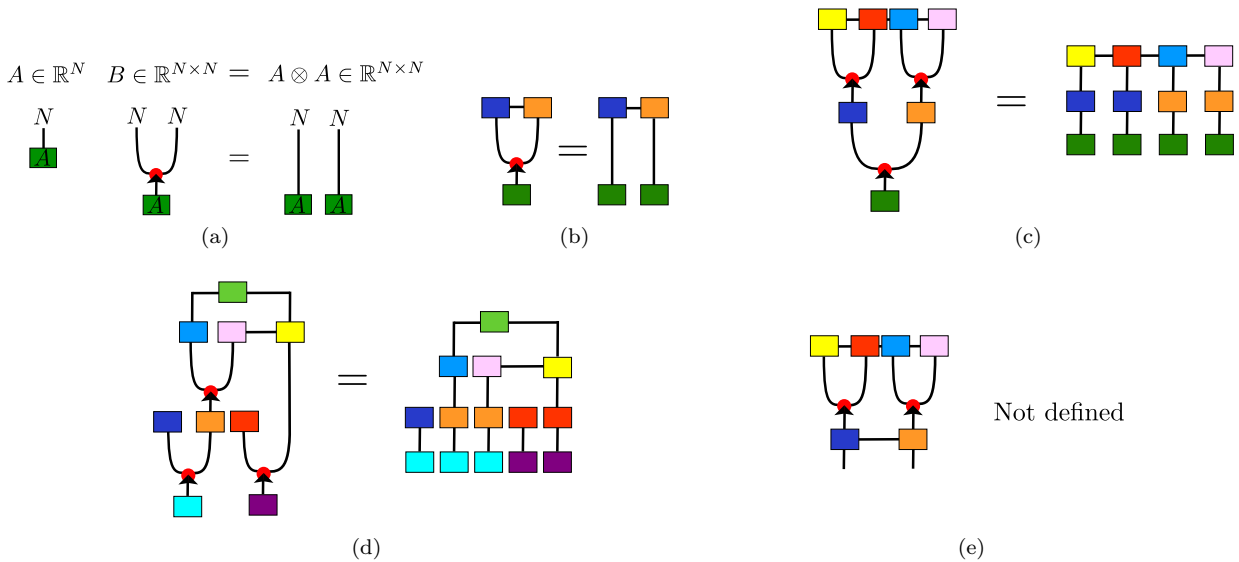


Figure 1: (a) Copy operation of a vector input A , resulting in a new tensor $B = A \otimes A$, where $B(i, j) = A(i)A(j)$. (b), (c) and (d) : Mapping of generalized tensor networks with copy operation to tensor networks with parameter sharing (cores with the same colors are identical). (e) This representation is not defined because we define the copy operation only for vectors. Adapted from I. Glasser, N. Pancotti, and J. I. Cirac. *From probabilistic graphical models to generalized tensor networks for supervised learning*. 2018. arXiv: 1806.05964 [quant-ph]. Copyright 2019 by Ivan Glasser, Nicola Pancotti, and J. Ignacio Cirac. CC BY 4.0

to get

$$X_0(h, w) = \varphi(X(h, w)).$$

Such representation of an image constitutes a tensor network with HW cores, none of them connected. See Figure 2 for illustration.

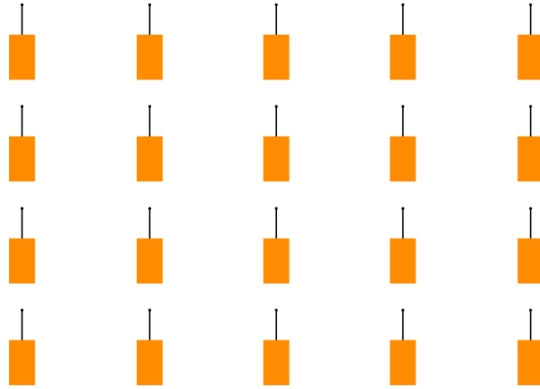


Figure 2: An image with height $H = H_0 = 4$ width $W = W_0 = 5$ represented as $4 \cdot 5 = 20$ vectors. This representation is a tensor network with none of the cores connected. $X_0(h, w)$ is depicted as the core in row h column w . Each core has one dangling edge since it's an order-1 tensor, i.e. a vector. Here we don't interpret the whole tensor network as an order-20 rank-1 tensor built from the outer product of the vectors, but as a collection of 20 vectors arranged on a grid.

Some choices of φ in the existing literature are:

- $\varphi(x) = \begin{bmatrix} \cos(\frac{\pi}{2}x) \\ \sin(\frac{\pi}{2}x) \end{bmatrix}$ - encodes the value x in a qubit. The components are nonnegative. It has ℓ_2 -norm equal to 1. It is used in (Grant et al. 2018), (Bhatia et al. 2019), (Stoudenmire and Schwab 2016), (Huggins et al. 2019).
- $\varphi(x) = \begin{bmatrix} x \\ 1 - x \end{bmatrix}$ - the components are nonnegative. Has ℓ_1 -norm equal to 1. Is used in (Miller 2019).
- $\varphi(x) = \begin{bmatrix} \cos^2(\frac{\pi}{2}x) \\ \sin^2(\frac{\pi}{2}x) \end{bmatrix}$ - the components are nonnegative. Is used in (Glasser, Pancotti, and Cirac 2018), and the authors say that the ℓ_1 -norm always being equal to 1 provides numerical stability.

- $\varphi(x) = \begin{bmatrix} 1 \\ x \end{bmatrix}$ - is used in (Novikov, Trofimov, and Oseledets 2016).

In light of the duality of tensor networks and discrete undirected probabilistic graphical models (see (Robeva and Seigal 2019), (Glasser, Pancotti, and Cirac 2018)), the second and third choices can be viewed as encoding a number as a binary probability distribution. In our work, we use

$$\varphi(x) = \nu \begin{bmatrix} \cos^2(\frac{\pi}{2}x) \\ \sin^2(\frac{\pi}{2}x) \end{bmatrix}, \quad (1)$$

where ν is some positive real number. The choice of ν is described in Section 5.1.

3.3 Entangled plaquette states

In quantum physics, **EPS** (entangled plaquette states) is a tensor network used for representing systems on a grid. (Glasser, Pancotti, and Cirac 2018) slightly modifies EPS to get a generalized tensor network, in which vectors arranged on a two-dimensional grid are contracted with tensor cores of parameters. In our work, we use the latter definition of EPS, which we will now describe.

Suppose K is a small positive integer called the **kernel size** (having the same meaning as kernel size in *Conv2d* function). Suppose $Q_{\text{in}}, Q_{\text{out}}$ are positive integers called the **quantum dimension size of input** and the **quantum dimension size of output**, respectively. Then an EPS with these kernel size and quantum dimensions sizes is parametrized with an order- $(1 + K^2)$ tensor

$$E \in \mathbb{R}^{Q_{\text{out}} \times Q_{\text{in}} \times \dots \times Q_{\text{in}}}$$

with one dimension of size Q_{out} and K^2 dimensions of size Q_{in} .

Now suppose $H_{\text{in}} \geq K, W_{\text{in}} \geq K$ are integers denoting the height and width of an input X_{in} consisting of $H_{\text{in}}W_{\text{in}}$ vectors, each of size Q_{in} arranged on a grid, i.e.

$$\forall h \in \{1, \dots, H_{\text{in}}\} \forall w \in \{1, \dots, W_{\text{in}}\} X_{\text{in}}(h, w) \in \mathbb{R}^{Q_{\text{in}}}.$$

Then applying the EPS parametrized by E to the input X_{in} produces an output $X_{\text{out}} = \text{eps}(E, X_{\text{in}})$ consisting of vectors of size Q_{out} arranged on a grid with height $H_{\text{out}} = H_{\text{in}} - K + 1$ and width $W_{\text{out}} = W_{\text{in}} - K + 1$ defined as

$$\forall h \in \{1, \dots, H_{\text{out}}\} \forall w \in \{1, \dots, W_{\text{out}}\} X_{\text{out}}(h, w) = \text{eps}(E, X_{\text{in}})(h, w) \in \mathbb{R}^{Q_{\text{out}}},$$

$$X_{\text{out}}(h, w, q_{\text{out}}) = \sum_{\substack{\forall \delta h \in \{0, \dots, K-1\} \\ \forall \delta w \in \{0, \dots, K-1\} \\ q_{\delta h, \delta w} \in \{1, \dots, Q_{\text{in}}\}}} E(q_{\text{out}}, q_{0,0}, q_{0,1}, \dots, q_{0,K-1}, q_{1,0}, \dots, q_{K-1,K-1}) \prod_{\delta h=0}^{K-1} \prod_{\delta w=0}^{K-1} X_{\text{in}}(h + \delta h, w + \delta w, q_{\delta h, \delta w}), \quad (2)$$

which can be written more compactly using tensor contraction operation as

$$X_{\text{out}}(h, w) = E \times_2 X_{\text{in}}(h + 0, w + 0) \times_3 X_{\text{in}}(h + 0, w + 1) \cdots \times_{1+K^2} X_{\text{in}}(h + K - 1, w + K - 1) \quad (3)$$

or using matricization $\text{mat}(E) \in \mathbb{R}^{Q_{\text{out}}, Q_{\text{in}}^{K^2}}$ of the tensor E , vectorization, outer product, and matrix multiplication as

$$X_{\text{out}}(h, w) = \text{mat}(E) \cdot \text{vec} \left(\bigotimes_{\delta h=0}^{K-1} \bigotimes_{\delta w=0}^{K-1} X_{\text{in}}(h + \delta h, w + \delta w) \right), \quad (4)$$

or using tensor network diagram in Figure 3 (for $K = 3$).

Also, an EPS parametrized by E applied to an input X_{in} is a generalized tensor network, as can be seen in Figure 4. Notice that application of an EPS to an input applies the same function to each $K \times K$ sliding window of the input. This provides two of our three desiderata mentioned in Section 1: *locality* and *parameter sharing*.

3.3.1 EPS as a backpropagatable layer

EPS can be implemented as a backpropagatable function/layer and be used in neural networks or other gradient descent based models. The formulas for forward pass are eqs. (2) to (4). Next we derive the backward pass formulas for derivatives. For

$$\frac{\partial \text{eps}(E, X_{\text{in}})(h, w)}{\partial X_{\text{in}}(h', w')} \in \mathbb{R}^{Q_{\text{out}} \times Q_{\text{in}}}$$

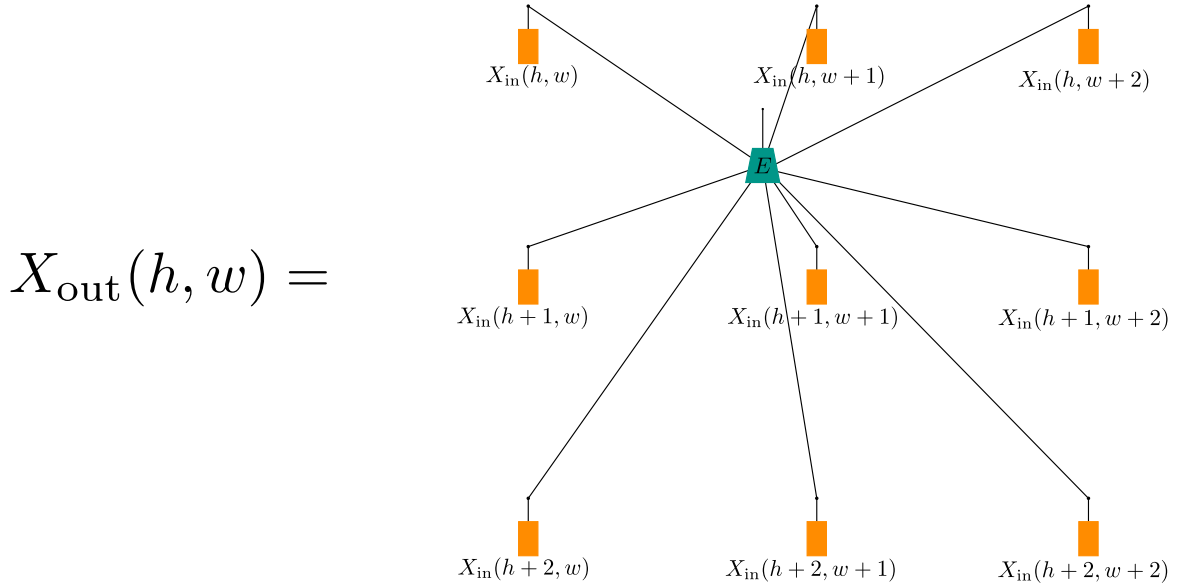


Figure 3: Visualization of one pixel of EPS's output with kernel size $K = 3$ as a tensor network. It is equivalent to eqs. (2) to (4).

we have

if $h' \in \{h, \dots, h + K - 1\} \wedge w' \in \{w, \dots, w + K - 1\}$, then

$$\frac{\partial \text{eps}(E, X_{\text{in}})(h, w)}{\partial X_{\text{in}}(h', w')} = E \times_2 X_{\text{in}}(h + 0, w + 0) \times_3 X_{\text{in}}(h + 0, w + 1) \cdots \times_{1+K^2} X_{\text{in}}(h + K - 1, w + K - 1),$$

for each pair of indices $(h + \delta h, w + \delta w)$ except $(h + \delta h = h', w + \delta w = w')$

otherwise

$$\frac{\partial \text{eps}(E, X_{\text{in}})(h, w)}{\partial X_{\text{in}}(h', w')} = 0,$$

and for

$$\frac{\partial \text{eps}(E, X_{\text{in}})(h, w)}{\partial E} \in \mathbb{R}^{Q_{\text{out}} \times Q_{\text{out}} \times Q_{\text{in}} \times \cdots \times Q_{\text{in}}}$$

we have

$$\frac{\partial \text{eps}(E, X_{\text{in}})(h, w)}{\partial E} = I \otimes \bigotimes_{\delta h=0}^{K-1} \bigotimes_{\delta w=0}^{K-1} X_{\text{in}}(h + \delta h, w + \delta w),$$

where $I \in \mathbb{R}^{Q_{\text{out}} \times Q_{\text{out}}}$ is the identity matrix.

3.4 Description of the whole model

The whole model is a (functional) composition of the preprocessing function φ described in Section 3.2, N EPSes described in Section 3.3 parametrized by tensors E_1, \dots, E_N , a linear layer (i.e. an affine function) parametrized by a matrix A and a vector b , and the softmax function. The whole model is defined by the following equations:

$$X_0(h, w) = \varphi(X(h, w)) \tag{5}$$

$$X_1 = \text{eps}(E_1, X_0) \tag{6}$$

$$X_2 = \text{eps}(E_2, X_1) \tag{7}$$

\vdots

$$X_N = \text{eps}(E_N, X_{N-1}) \tag{8}$$

$$\ln \hat{p}(y = \ell | X) = (A \cdot \text{vec}(X_N) + b)_\ell \tag{9}$$

$$p(y = \ell | X) = \text{softmax} \left(\begin{bmatrix} \ln \hat{p}(y = 1 | X) \\ \ln \hat{p}(y = 2 | X) \\ \vdots \\ \ln \hat{p}(y = L | X) \end{bmatrix} \right)_\ell = \frac{\hat{p}(y = \ell | X)}{\sum_{\ell'=1}^L \hat{p}(y = \ell' | X)}, \tag{10}$$

where L is the number of labels an image can have. See a visualization of this chain of transformations in Figure 5. The original input image X is represented as a tensor of shape $H_0 \times W_0$. For each $n \in \{1, \dots, N\}$, the n -th intermediate

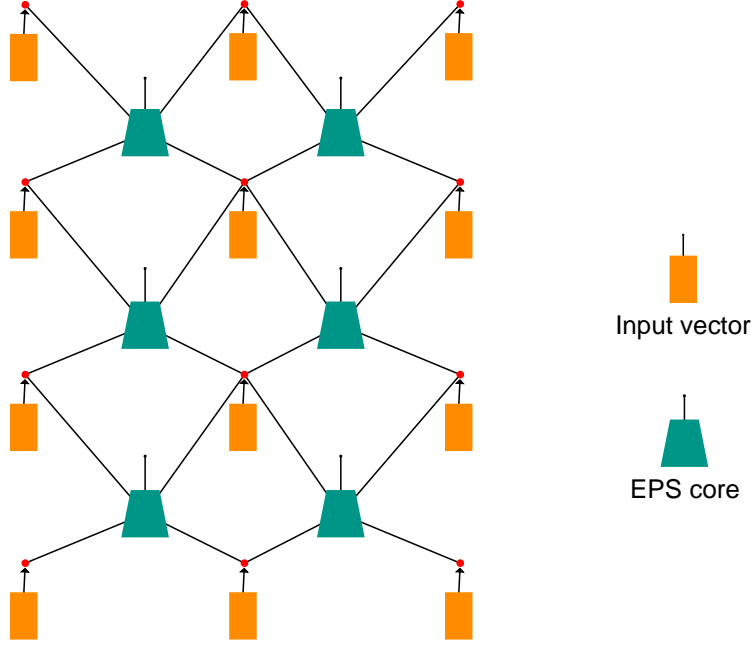


Figure 4: An EPS parametrized by E applied to an input X_{in} is a generalized tensor network with all teal cores being identical and equal to E . In this case, we have kernel size $K = 2$, input height $H_{\text{in}} = 4$, input width $W_{\text{in}} = 3$. For each of the input vectors, the copy operation produces copies of it for each of the output vectors it affects. The copies are contracted with the corresponding teal cores.

representation X_n can be represented as a tensor of shape $H_n \times W_n \times Q_n$, where the quantum dimension size Q_n is determined by the size of the EPS E_n and height and width are determined by

$$\begin{aligned} H_n &= H_{n-1} - K_n + 1, \\ W_n &= W_{n-1} - K_n + 1, \end{aligned}$$

where K_n is the kernel size of the n -th EPS.

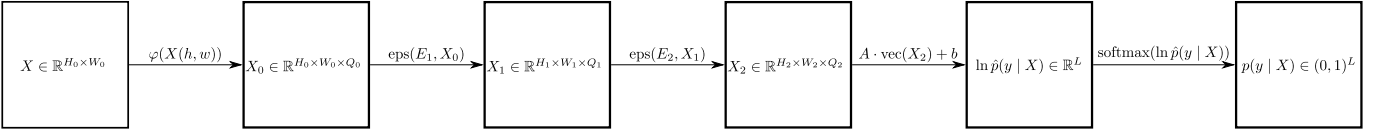


Figure 5: Diagram of the whole model for the number of EPSes $N = 2$. Squares are representations of an input. Edges are functions, some of which are parametrized. The last square represents the predicted probabilities of labels.

In principle, the affine function parametrized by A and b can be replaced with another differentiable possibly parametrized function, for example another tensor network.

Just like a single EPS applied to an input is a generalized tensor network, a composition of EPSes applied to an input is also a generalized tensor network, as shown in Figure 6. Also, a composition of EPSes, when not applied to an input, can be thought of as a non-generalized tensor network, as shown in Figure 7.

3.5 Optimization

We initialize parameters E_1, \dots, E_N and A, b of the model randomly (for initialization details see Section 5.1). Recall from Figure 7 that an EPSes composition can be thought of as a tensor network representing a high order tensor. For the N EPSes, denote this tensor as $\text{TN}(E_1, \dots, E_N)$ (here TN stands for “tensor network”). Recall from eqs. (5) to (10) that the predictions of our model are probabilities $p(y | X)$ which depend on the model’s parameters. Let $\lambda \geq 0$ be the regularization coefficient. To train the model, at each iteration we sample M images $X^{(1)}, \dots, X^{(M)}$ and their labels $y^{(1)}, \dots, y^{(M)}$ from the training dataset and use Adam optimizer (Kingma and Ba 2014) with either the objective

$$\underset{E_1, \dots, E_N, A, b}{\text{minimize}} \lambda \left(\|\text{TN}(E_1, \dots, E_N)\|_{\text{fro}}^2 + \|A\|_{\text{fro}}^2 \right) + \frac{1}{M} \sum_{m=1}^M -\ln p\left(y^{(m)} | X^{(m)}\right), \quad (11)$$

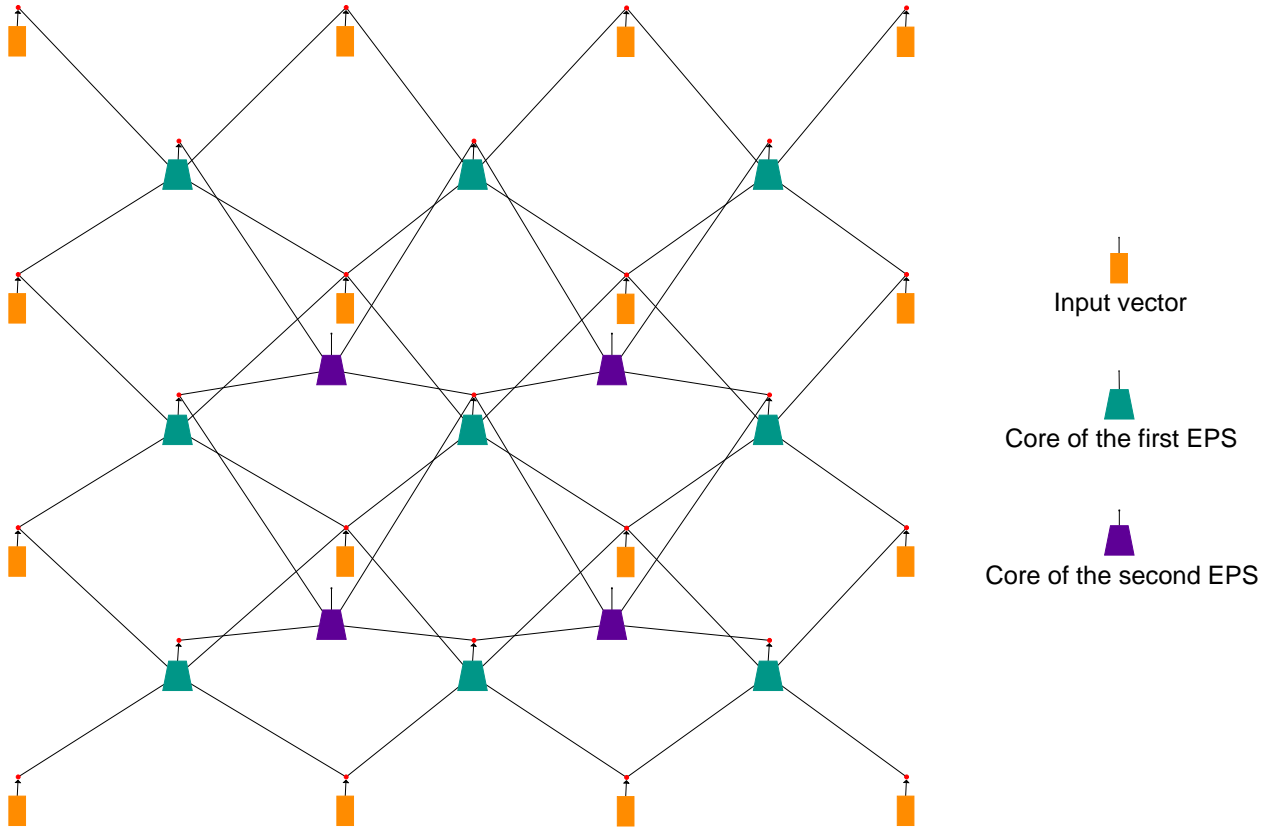


Figure 6: $X_2 = \text{eps}(E_2, \text{eps}(E_1, X_0))$ visualized as a generalized tensor network diagram. In this case we have $H_0 = W_0 = 4, K_1 = 1, H_1 = W_1 = 3, K_2 = 2, H_2 = W_2 = 2$. Orange cores are vectors of the zeroth representation X_0 . Teal cores are cores of the first EPS, and each of them is equal to E_1 . Purple cores are cores of the second EPS, and each of them is equal to E_2 . The diagram has 4 dangling edges because in this case, the second EPS outputs 4 vectors.

or the objective

$$\underset{E_1, \dots, E_N, A, b}{\text{minimize}} \quad \lambda \left(\|E_1\|_{\text{fro}}^2 + \dots + \|E_N\|_{\text{fro}}^2 + \|A\|_{\text{fro}}^2 \right) + \frac{1}{M} \sum_{m=1}^M -\ln p \left(y^{(m)} \mid X^{(m)} \right). \quad (12)$$

We calculate the objective’s gradient with respect to the model’s parameters using backpropagation via Pytorch (Paszke et al. 2019) autograd. We train the model in iterations, periodically evaluating it on the validation dataset, and take the model with the best validation accuracy as the final output of the training process.

4 Experiments

4.1 MNIST

We tested our model with just one EPS, $\nu = 0.5$ in eq. (1), $K_1 = 4, Q_1 = 4, \text{lr} = 3 \cdot 10^{-3}, \lambda = 0$ in eq. (11) on MNIST dataset with 50000/10000/10000 training/validation/test split. We got 98.75% test accuracy. MNIST is considered relatively easy and doesn’t represent modern computer vision tasks (Xiao, Rasul, and Vollgraf 2017b).

4.2 FashionMNIST

FashionMNIST (Xiao, Rasul, and Vollgraf 2017a) is a dataset fully compatible with MNIST: it contains 70000 grayscale 28×28 images. Each image belongs to one of 10 classes of clothes. The goal is to predict the correct class. We split 70000 images into 50000/10000/10000 training/validation/test split and experimented with models with one, two, and three EPSes. We didn’t experiment with more EPSes, because more EPSes increased overfitting and decreased validation accuracy. The best results (chosen by validation accuracy before being evaluated on the test dataset) are shown in Table 1. More experiments and our discussion about how various hyperparameters affect optimization and generalization of our model are presented in Section 5.

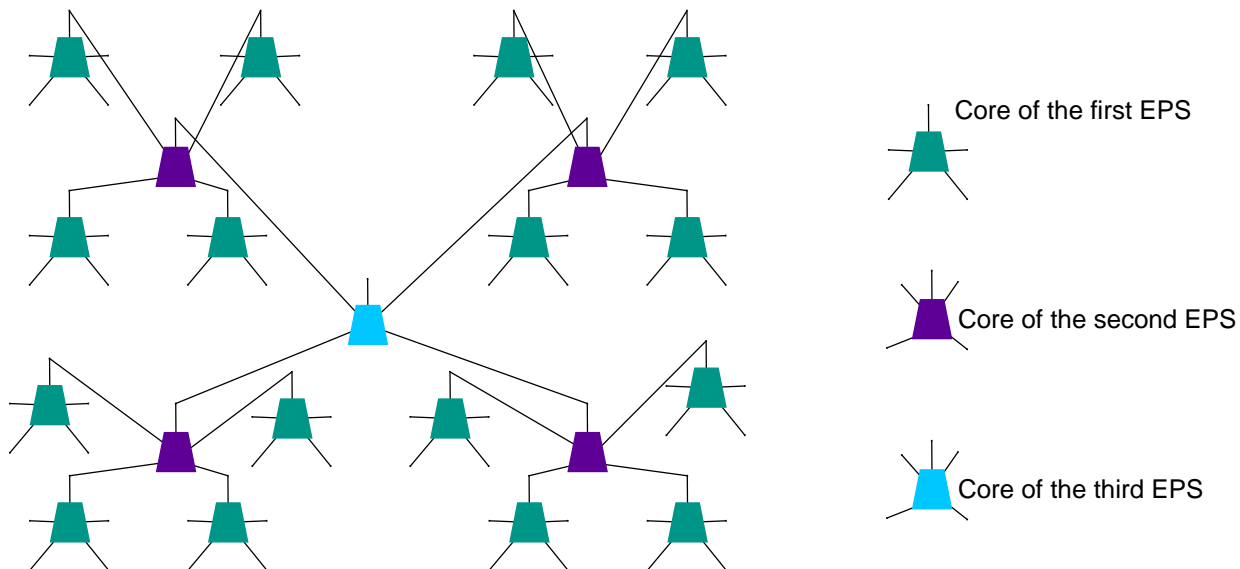


Figure 7: A diagram showing how a composition of EPSes, when not applied to an input, can be thought of as a tensor network, which represents a high order tensor. In this diagram, we have kernel sizes $K_1 = K_2 = K_3 = 2$. Cores of the three EPSes are colored teal, purple, and light blue, respectively. For each of the three colors, all cores of that color are equal to each other. Each dangling edge of each teal core has dimension size Q_0 . The only dangling edge of the light blue core has dimension size Q_3 . This tensor network represents an order- $(4^3 + 1)$ tensor. To get one vector of the output of the third EPS, take 4^2 vectors of a 4×4 window of the input X_0 , copy some of them in the right way to get 4^3 vectors, and contract them with this tensor network.

5 How hyperparameters affect optimization and generalization

All experimental findings listed in this section have only been tested on one dataset and with some of the hyperparameters fixed. These preliminary findings might not replicate on other datasets or with other configurations of hyperparameters.

5.1 Initialization of the model and scaling of the input

Suppose our model has N EPSes with kernel sizes K_1, \dots, K_N . Let $c > 0$ be a positive real number. Then

$$A \cdot \text{vec}(\text{eps}(E_N, \dots \text{eps}(E_2, \text{eps}(E_1, cX_0)) \dots)) = c^{K_1^2 K_2^2 \dots K_N^2} A \cdot \text{vec}(\text{eps}(E_N, \dots \text{eps}(E_2, \text{eps}(E_1, X_0)) \dots)) \quad (13)$$

and

$$A \cdot \text{vec}(\text{eps}(E_N, \dots \text{eps}(E_2, \text{eps}(cE_1, X_0)) \dots)) = c^{K_2^2 \dots K_N^2} A \cdot \text{vec}(\text{eps}(E_N, \dots \text{eps}(E_2, \text{eps}(E_1, X_0)) \dots)) \quad (14)$$

Since $K_1^2 K_2^2 \dots K_N^2$ can get very large (e.g. 576 for $K_1 = 4, K_2 = 3, K_3 = 2$), it follows that if the constant ν in the input preprocessing function

$$\varphi(x) = \nu \begin{bmatrix} \cos^2(\frac{\pi}{2}x) \\ \sin^2(\frac{\pi}{2}x) \end{bmatrix} \quad (1)$$

is chosen slightly larger than optimal, eq. (13) might easily get infinities in floating point arithmetic, and if it's chosen slightly smaller than optimal, eq. (13) might easily become all zeros, and the model's output will stop depending on anything except the bias b .

The same is true in a slightly lesser degree for scaling of initial values of E_1, \dots, E_N , especially for the earlier EPSes, as shown in eq. (14). Also, if for a chosen ν and chosen initialization of the EPSes, the values in

$$A \cdot \text{vec}(\text{eps}(E_N, \dots \text{eps}(E_2, \text{eps}(E_1, X_0)) \dots))$$

have large standard deviation, then the values in the output of the whole model

$$A \cdot \text{vec}(\text{eps}(E_N, \dots \text{eps}(E_2, \text{eps}(E_1, X_0)) \dots)) + b$$

will have large standard deviation as well, which might lead to initial negative log likelihood being high. (Karpathy 2019) recommends initializing neural networks for classification in such a way that initially the loss has the best possible value given that your model is allowed to know the proportion of labels in the datasets, but hasn't been allowed to train yet. For example, if you have 10 possible labels with equal number of samples, a perfectly calibrated

Model	Accuracy	Parameter count
One EPS $K_1=4$, $Q_1=4$, $\nu=0.5$, $E_1 \sim \mathcal{N}(\mu=0, \sigma=0.25)$, $A, b \sim U[-(H_1 W_1 Q_1)^{-0.5}, -(H_1 W_1 Q_1)^{0.5}]$, lr= $3 \cdot 10^{-3}$, $\lambda=0$, eq. (11)	89.38%	$2.9 \cdot 10^5$
Two EPSes, $K_1=4, Q_1=4, K_2=3, Q_2=6$, $\nu \approx 1.46$, EPSes initialized from $\mathcal{N}(\mu=0, \sigma=Q_{\text{in}}^{-0.5K^2})$, $A \sim \mathcal{N}(\mu=0, \sigma=0.25(H_2 W_2 Q_2)^{-0.5})$, $b \sim U[-(H_2 W_2 Q_2)^{-0.5}, (H_2 W_2 Q_2)^{-0.5}]$, lr= $1.11 \cdot 10^{-4}$, $\lambda=10^{-2}$, eq. (12)	87.65%	$1.8 \cdot 10^6$
Three EPSes, $K_1=4, Q_1=4, K_2=3, Q_2=12, K_3=2, Q_3=24$, $\nu \approx 1.46$, EPSes initialized i.i.d. normally and rescaled to make $\text{std}(X_1)=\text{std}(X_2)=\text{std}(X_3)=1$, $A \sim \mathcal{N}(\mu=0, \sigma=0.25(H_2 W_2 Q_2)^{-0.5})$, $b \sim U[-(H_3 W_3 Q_3)^{-0.5}, (H_3 W_3 Q_3)^{-0.5}]$, lr= 10^{-7} , $\lambda=10^{-1}$, eq. (11)	75.94%	$4 \cdot 10^6$
DENSER ensembling	95.26%	?
GoogleNet + Linear SVC	93.7%	$6.8 \cdot 10^6$
VGG16	93.5%	$2.6 \cdot 10^7$
CNN: 5x5 conv -> 5x5 conv -> linear -> linear	91.6%	$3.3 \cdot 10^6$
AlexNet + Linear SVC	89.9%	$6.2 \cdot 10^7$
Matrix tensor train in snake pattern (Glasser 2019)	89.2%	?
Multilayer perceptron	88.33%	$2.3 \cdot 10^5$

Table 1: Comparison of our best models (top 3 rows) consisting of 1, 2, and 3 EPSes plus a linear layer, respectively, with best existing models on FashionMNIST dataset, where best is determined by the combination of test accuracy and parameter count. Our model with one EPS wins against existing models with similar parameter count. Adding more EPSes makes test accuracy worse due to overfitting. All 3 of our models eventually reach nearly 100% accuracy if not stopped early. We train all models in our article with batch size 128.

model that is ignorant about the images should have negative log likelihood equal to $\ln 10 \approx 2.3$. We conjecture that if the model starts with negative log likelihood much higher than this value, problems with the optimization process might occur.

One way we tried to overcome this difficulty was by using *He initialization* (He et al. 2015) of EPSes

$$E \sim \mathcal{N}(\mu = 0, \sigma = Q_{\text{in}}^{-0.5K^2}). \quad (15)$$

The rationale for this initialization is that if the components of $E \in \mathbb{R}^{Q_{\text{out}} \times Q_{\text{in}} \times \dots \times Q_{\text{in}}}$ are distributed i.i.d. with zero mean and variance α^2 , and if the components of $\omega \in \mathbb{R}^{Q_{\text{in}} \times \dots \times Q_{\text{in}}}$ are distributed i.i.d. with mean μ and variance σ^2 , then, applying the EPS E similar to eq. (4), we have

$$\mathbb{E}[\text{mat}(E) \cdot \text{vec}(\omega)] = 0,$$

$$\text{Var}[\text{mat}(E) \cdot \text{vec}(\omega)] = Q_{\text{in}}^{K^2} \alpha^2 (\sigma^2 + \mu^2) I.$$

Note that the input ω having i.i.d. coordinates is not necessarily true in the real scenario, but still, we might try to initialize the EPSes using He initialization eq. (15). In this case, we choose such value for ν as to have the components of the vector

$$\omega_0(h, w) = \text{vec} \left(\bigotimes_{\delta h=0}^{K_1-1} \bigotimes_{\delta w=0}^{K_1-1} X_0(h + \delta h, w + \delta w) \right),$$

(which appears in eq. (4)) (here the letter ω is chosen for its similarity to the letter w , which is already taken, because ω is a “window” of size $K_1 \times K_1$), have empirical mean μ and empirical standard deviation σ (over the whole training dataset) satisfy $\mu^2 + \sigma^2 = 1$. For example, on FashionMNIST with our choice of φ , the value $\nu \approx 1.46$ satisfies this criterion, and that’s the value we use in 2 out of 3 experiments in Table 1.

However, empirically we’ve seen that with this initialization with 2 EPSes, the empirical standard deviation (over the whole training dataset) of the second intermediate representation $\text{std}(X_2)$ sometimes (depending on the random seed) is magnitudes larger or smaller than 1. If it’s large, this leads to initial negative log likelihood loss being high, which is bad. That’s why we devised another initialization scheme: while choosing ν the same way described earlier, we first initialize components of each EPS E_n from the standard normal distribution and then rescale the EPS by the number required to make empirical standard deviation (over the whole training dataset) of its output X_n equal to 1. From now on in our work, we will call this initialization scheme *empirical unit std of intermediate representations initialization*. You can see a visualization of its effects in Figure 8.

5.2 Other hyperparameters

- Figure 9 discusses how high learning rate leads to less overfitting.
- Figure 10 discusses how we accidentally got the best result with one EPS by setting a very small ν .
- Figure 11 discusses how the ℓ_2 regularization coefficient λ affects training.

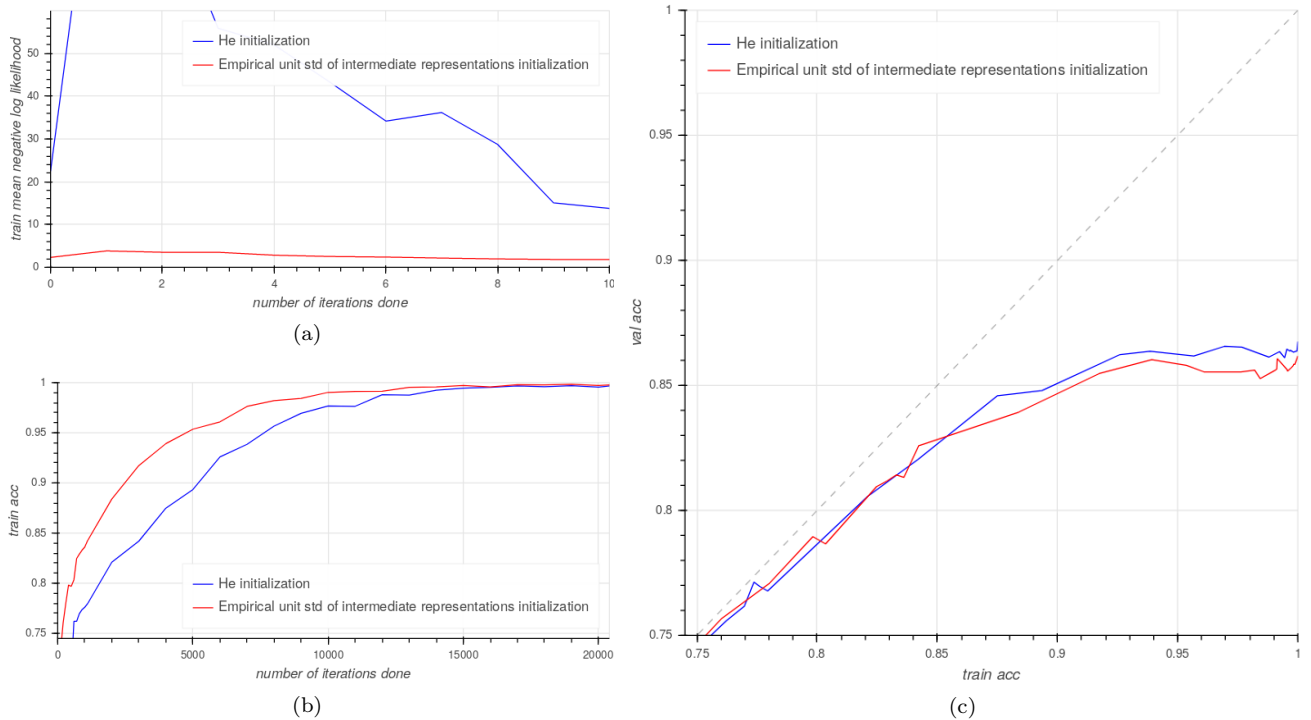


Figure 8: Comparison of He initialization and empirical unit std of intermediate representations initialization. (a) shows that He initialization suffers from high initial loss. (b) shows that empirical unit std of intermediate representations initialization trains faster. Unfortunately (c) shows that this didn’t lead to less overfitting. The model consists of 2 EPSes with $K_1=3, Q_1=4, K_2=3, Q_2=6, lr = 4 \cdot 10^{-5}, \lambda = 10^{-2}$, and the objective function eq. (11).

6 Conclusion

We have shown how an EPS (entangled plaquette states) can be implemented as a backpropagatable function/layer. We devised a novel tensor regression based model called DCTN (deep convolutional tensor network) built from a composition of EPSes, which can be used for image classification. In principle, it can be used in any task where DCNNs (deep convolutional neural networks) are used. Like DCNNs, it has locality, parameter sharing, and is deep. We have tested it on FashionMNIST dataset and found that while a shallow version performs well for its small parameter count, making it deep makes it overfit more and thus perform worse. This suggests that composing EPSes doesn’t seem promising. Since a shallow version performed well, it might be interesting to study using EPS as a layer in neural networks. We have discussed how hyperparameters affect training and generalization. Our understanding of this is poor. For example, we got our best model by scaling down the multiplier ν used in the input preprocessing function. It’s important to study and understand why it helped fight overfitting. Our code can be accessed at <https://github.com/philip-bl/dctn>.

References

- [1] A. S. Bhatia et al. “Matrix Product State–Based Quantum Classifier”. In: *Neural computation* 31.7 (2019), pp. 1499–1517.
- [2] J. Biamonte and V. Bergholm. “Tensor networks in a nutshell”. In: *arXiv preprint arXiv:1708.00006* (2017).
- [3] J. C. Bridgeman and C. T. Chubb. “Hand-waving and interpretive dance: an introductory course on tensor networks”. In: *Journal of Physics A: Mathematical and Theoretical* 50.22 (2017), p. 223001.
- [4] A. Cichocki, A. Phan, et al. “Tensor networks for dimensionality reduction and large-scale optimizations: Part 2 applications and future perspectives”. In: *Foundations and Trends in Machine Learning* 9.6 (2017), pp. 431–673.
- [5] A. Cichocki, N. Lee, et al. “Low-rank tensor networks for dimensionality reduction and large-scale optimization problems: Perspectives and challenges part 1”. In: *arXiv preprint arXiv:1609.00893* (2016).
- [6] N. Cohen, O. Sharir, and A. Shashua. “On the expressive power of deep learning: A tensor analysis”. In: *Conference on Learning Theory*. 2016, pp. 698–728.
- [7] H. G. Ehrbar. “Graph notation for arrays”. In: *ACM SIGAPL APL Quote Quad* 31.3 (2000), pp. 13–26.
- [8] I. Glasser, N. Pancotti, and J. I. Cirac. *From probabilistic graphical models to generalized tensor networks for supervised learning*. 2018. arXiv: 1806.05964 [quant-ph].
- [9] E. Grant et al. “Hierarchical quantum classifiers”. In: *npj Quantum Information* 4.1 (2018), pp. 1–8.

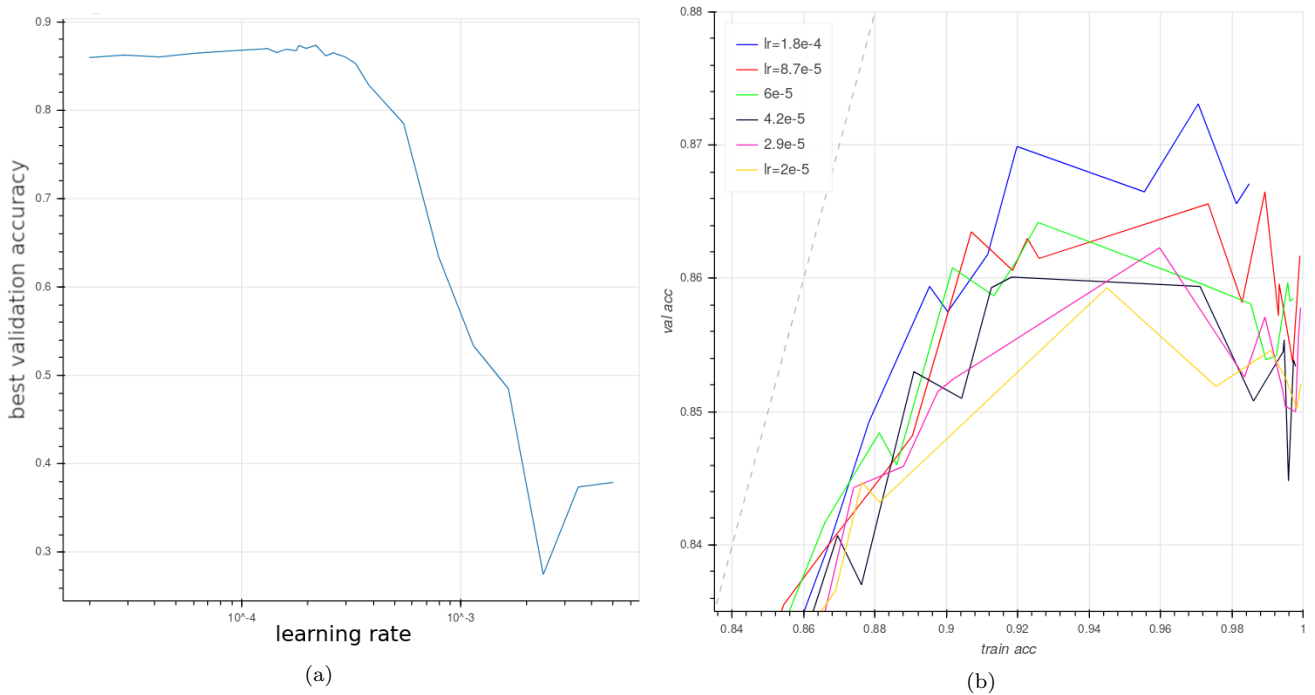


Figure 9: As can be seen in (a), too large learning rate causes training to not converge. However (b) shows that large but not too large learning rate slightly reduces overfitting. This is in line with folk understanding of how learning rate affects training in deep learning. The model has 2 EPSes with $K_1=4, Q_1=4, K_2=3, Q_2=6, \lambda = 10^{-2}$, the objective function eq. (11), and empirical unit std of intermediate representations initialization.

- [10] K. He et al. “Delving deep into rectifiers: Surpassing human-level performance on imagenet classification”. In: *Proceedings of the IEEE international conference on computer vision*. 2015, pp. 1026–1034.
- [11] W. Huggins et al. “Towards quantum machine learning with tensor networks”. In: *Quantum Science and technology* 4.2 (2019), p. 024001.
- [12] Karpathy. *A Recipe for Training Neural Networks*. 2019. URL: <https://karpathy.github.io/2019/04/25/recipe> (visited on 05/25/2020).
- [13] D. P. Kingma and J. Ba. “Adam: A method for stochastic optimization”. In: *arXiv preprint arXiv:1412.6980* (2014).
- [14] D. Liu et al. “Machine learning by unitary tensor network of hierarchical tree structure”. In: *New Journal of Physics* 21.7 (2019), p. 073059.
- [15] J. Miller. *TorchMPS*. <https://github.com/jemisjoky/torchmps>. 2019.
- [16] A. Novikov, M. Trofimov, and I. Oseledets. “Exponential machines”. In: *arXiv preprint arXiv:1605.03795* (2016).
- [17] R. Orús. “A practical introduction to tensor networks: Matrix product states and projected entangled pair states”. In: *Annals of Physics* 349 (2014), pp. 117–158.
- [18] PapersWithCode. *Browse the state-of-the-art in machine learning*. 2020. URL: <https://paperswithcode.com/sota> (visited on 05/23/2020).
- [19] A. Paszke et al. “PyTorch: An Imperative Style, High-Performance Deep Learning Library”. In: *Advances in Neural Information Processing Systems 32*. Ed. by H. Wallach et al. Curran Associates, Inc., 2019, pp. 8024–8035. URL: <http://papers.nips.cc/paper/9015-pytorch-an-imperative-style-high-performance-deep-learning-library.pdf>.
- [20] E. Robeva and A. Seigal. “Duality of graphical models and tensor networks”. In: *Information and Inference: A Journal of the IMA* 8.2 (2019), pp. 273–288.
- [21] E. M. Stoudenmire and D. J. Schwab. *Supervised Learning with Quantum-Inspired Tensor Networks*. 2016. arXiv: 1605.05775 [stat.ML].
- [22] H. Xiao, K. Rasul, and R. Vollgraf. “Fashion-mnist: a novel image dataset for benchmarking machine learning algorithms”. In: *arXiv preprint arXiv:1708.07747* (2017).
- [23] H. Xiao, K. Rasul, and R. Vollgraf. *FashionMNIST readme*. 2017. URL: <https://github.com/zalando-research/fashion-mnist/blob/master/README.md> (visited on 05/24/2020).

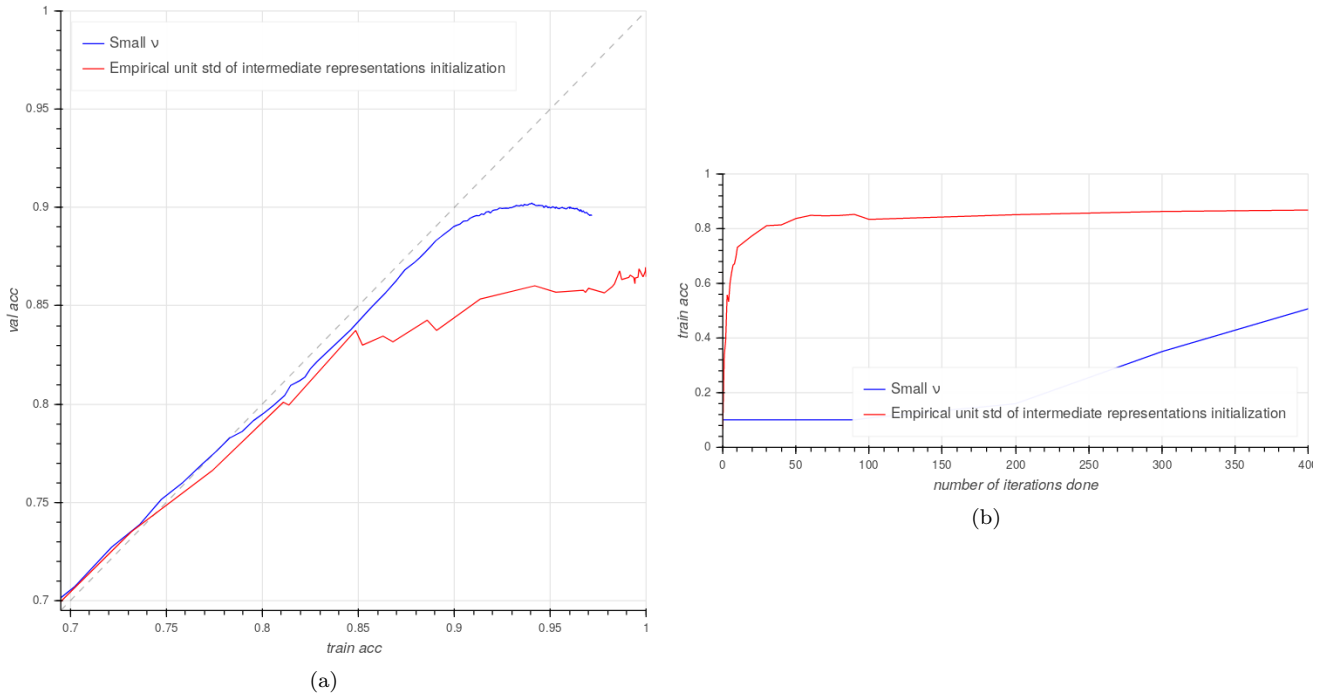


Figure 10: The plot (a) shows how a model we made by accidentally altering hyperparameters achieves better generalization. But it trained 960 times slower (b). Both models have one EPS with $K_1=4, Q_1=4, lr=3 \cdot 10^{-3}, \lambda = 0, A, b \sim U[-0.02, 0.02]$. The difference is in the choice of ν and in initialization of EPSes. The blue model is the model from the first row of Table 1. It has $\nu=0.5$ and its intermediate representations have standard deviations $\text{std}(X_1) \approx 1.7 \cdot 10^{-6}, \text{std}(A \cdot \text{vec}(X_1)) \approx 1.1 \cdot 10^{-6}$. The red model uses empirical unit std of intermediate representations initialization and has $\nu \approx 1.46, \text{std}(X_1)=1$. Notice that the standard deviation of the output of linear layer of the blue model, if we don't add the bias b , is very small compared to the standard deviation of the bias b . We speculate that this is probably the reason of much better generalization. It important to understand why the blue model's initialization and the choice of ν worked so well and figure out how to achieve it with more EPSes.

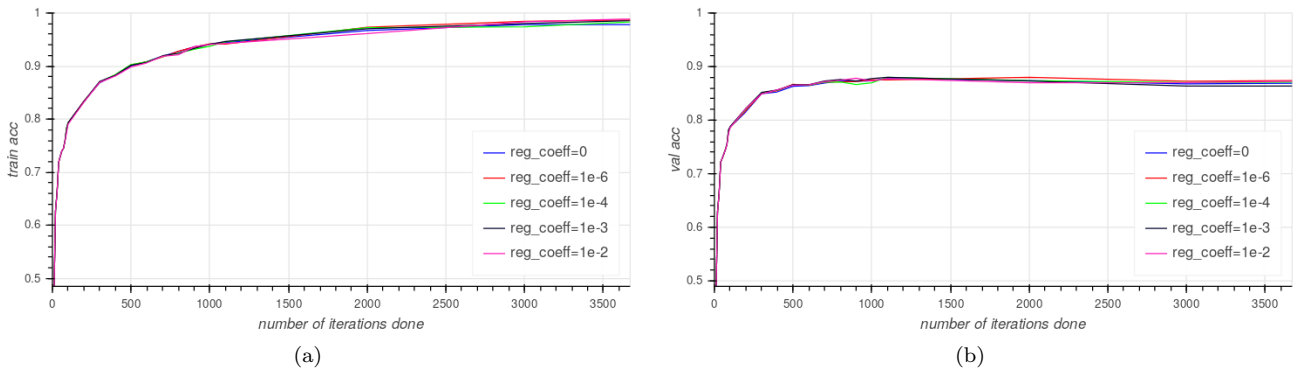


Figure 11: Two plots showing training dynamic depending on the ℓ_2 regularization coefficient λ . Neither training speed, nor validation accuracy seems to depend on λ . The model has 2 EPSes with $K_1=4, Q_1=4, K_2=3, Q_2=6, lr=1.11 \cdot 10^{-4}$, He initialization of EPSes, $A \sim \mathcal{N}(\mu=0, \sigma=0.25(H_2W_2Q_2)^{-0.5}), b \sim U[-(H_2W_2Q_2)^{-0.5}, (H_2W_2Q_2)^{-0.5}]$, and eq. (11) objective function.